



Proceeding Paper

Analysis of Optical Properties and Radiative Forcing of Different Aerosol Types in Wuhan [†]

Xin Nie

College of New Energy and Materials, Northeast Petroleum University, Daqing 163318, China; niexin@wust.edu.cn; Tel.: +86-17386183202

[†] Presented at the 6th International Electronic Conference on Atmospheric Sciences, 15–30 October 2023; Available online: <https://ecas2023.sciforum.net/>.

Abstract: The optical and radiative properties of aerosols are governed by their types. In this paper, the optical and radiative properties of different aerosol types in Wuhan, China, have been inverted and investigated using the collected PM_{2.5} samples. The results show that PM_{2.5} (average mass concentration about 31.25 µg/m³) is mainly contributed by sulfate (SO₄) and organic carbon (OC) (22% and 52%, respectively), while aerosol optical depth (AOD, average about 0.28) is mainly contributed by SO₄ and black carbon (EC) (22% and 19%, respectively). SO₄ and nitrate (NO₃) have a negative radiative forcing at the top of the atmosphere (TOA) and a cooling effect, while OC and EC have a positive radiative forcing and a heating effect. Moreover, EC has the most significant effect on the radiative forcing in Wuhan, contributing up to 61% and 73% at the bottom of the atmosphere (BOA) and atmosphere (ATM), respectively, while contributing up to 75% to the atmospheric heating rate (about 1–2 K/day).

Keywords: aerosol optical properties; PM_{2.5}; direct radiative forcing; atmospheric heating rate

1. Introduction

Aerosols are one of the most influential factors in the Earth system, as an important component of the atmosphere. Aerosols affect the Earth's energy balance via direct and indirect radiative effects, the direct radiative effect being due to the aerosol absorption and scattering of solar radiation, and the indirect radiative effect coming from the fact that aerosols act as cloud condensation nuclei changing the life cycle and physical properties of clouds [1]. Additionally, aerosols can affect human health as respirable particulate matter and reduce visibility in highly polluted regions [2]. However, these effects are usually highly uncertain because aerosols are much more varied in composition and much more heterogeneous in spatial and temporal distributions than greenhouse gases, and there is still a lack of sufficient aerosol information at larger spatial and temporal scales [3].

For decades, recognition of this fact has motivated tremendous efforts, and a great number of in situ measurements and optical remote sensing works have provided valid information on the optical and microphysical properties of aerosols, which have contributed to reducing the uncertainty of aerosols in the global and regional climate system [4,5]. Based on a large number of observation data, various aerosol classification methods have been developed to assess the global and regional distribution characteristics of aerosols in order to improve the level of understanding of aerosols. For example, using a combination of aerosol optical depth (AOD) and Angstrom exponent (AE) index to achieve aerosol classification, or combining AE with single scattering albedo (SSA), as well as using parameters such as AROD [6–8]. Moreover, numerous studies have discussed in depth the components and sources of regional aerosols. Hammer et al. have assessed the trends in global particulate matter concentrations using methods such as satellites and modeling [4]. Studies in China, India, and Europe have also revealed sources and drivers of



Citation: Nie, X. Analysis of Optical Properties and Radiative Forcing of Different Aerosol Types in Wuhan. *Environ. Sci. Proc.* **2023**, *27*, 31. <https://doi.org/10.3390/ecas2023-16347>

Academic Editor: Patricia Quinn

Published: 27 November 2023



Copyright: © 2023 by the author. Licensee MDPI, Basel, Switzerland. This article is an open access article distributed under the terms and conditions of the Creative Commons Attribution (CC BY) license (<https://creativecommons.org/licenses/by/4.0/>).

particulate matter at smaller spatial scales [9–11]. Source analysis of aerosols in Beijing and Wuhan reveals the dominant influence of traffic and industrial emissions [2,12–15]. Studies have shown that different aerosol types may have different or even opposite radiative effects [16–18]. Therefore, improving the level of understanding of the optical properties and radiative effects of different aerosol types can effectively limit the aerosol direct and indirect radiative forcing and enhance the accuracy of the assessment of aerosol environmental and climate effects.

Wuhan is a major city in central China with more serious pollution and higher aerosol loading. It is mainly attributed to the rapidly growing industry and the consequent increase in energy consumption in Wuhan. The high ambient humidity and stable planetary boundary layer also limit the pollutant dispersion, which further increases the aerosol loading. Although considerable studies have investigated the composition, sources, and distribution of aerosols in Wuhan, the aerosol radiative effect depends more on the combined contribution of multiple aerosol types, and up to now, there are no relevant studies involving the radiative effects of different aerosol types and their relative contributions in Wuhan [2,13–15]. In this study, an in situ measurement experiment of atmospheric aerosols is carried out in Wuhan. The mass concentrations (MC) of different aerosol types are investigated and analyzed by the collected PM_{2.5} samples, and the radiative forcing and atmospheric heating rates of aerosol types are subsequently simulated and discussed based on the inverted aerosol optical properties. This paper aims to reveal the radiative properties of different aerosol types in Wuhan and to limit the uncertainty of aerosol properties and radiative forcing in Wuhan.

2. Materials and Methods

2.1. In Situ Measurement of Aerosols

The sampling site is located at Baishazhou Avenue in Wuhan, China, as shown in Figure 1. With a total population of about 17 million, developed industry, and high car ownership, the aerosols over Wuhan are mainly from various anthropogenic sources. In this study, nine sets (days) of PM_{2.5} data collected during 2021 are used, with a sampling duration of 20 h or 24 h. The equipment and operation of the experiment are described in detail in the earlier study [19], and the sampling results are shown in Figure 2. The results show that the MC of PM_{2.5} ranges from 26~37 µg/m³, with mean values of about 31.25 µg/m³, and SO₄²⁻ and NO₃⁻ range from 0.463~1.04 µg/m³ and 5.015~8.19 µg/m³, with mean values of about 6.94 µg/m³ and 0.67 µg/m³, respectively. The MC of organic carbon (OC) and elemental carbon (EC) range from 9.22~16.31 µg/m³ and 0.95~2.03 µg/m³, with mean values of about 11.82 µg/m³ and 1.63 µg/m³, respectively. PM_{2.5} is mainly contributed by SO₄ and OC, accounting for about 22% and 52%, respectively. Several studies show that water-soluble ions such as SO₄²⁻ and NO₃⁻ in Wuhan mainly originate from vehicle exhaust emissions and organic matter combustion, while EC mainly comes from industrial production and coal-fired heating. In addition, the burning of straw in the surrounding countryside is also one of the main sources of EC, while OC comes more from the incomplete combustion of biomass and fossil fuels [14,15].

2.2. Aerosol Optical Properties

In this study, the Optical Properties of Aerosols and Clouds (OPAC) model is used to implement the calculation of aerosol optical properties [20]. This package provides aerosol optical properties at 61 wavelengths between 0.3 µm and 40 µm and 8 relative humidities and is widely used for the calculation and inversion of the optical properties of mixed aerosols with multiple components. The core idea of the inversion is to calculate the AOD by inputting the number density of aerosols and matching it with the observation data. Specifically, the corresponding number densities are first calculated from the MC of the different aerosol types obtained using sampling. Subsequently, parameters such as number density, height profile, and relative humidity are input into the OPAC program, and the aerosol optical properties such as AOD, SSA, and asymmetry factor (ASY) are

calculated and recorded. Finally, the AOD is compared with the observation data, and if the relative error is less than 10%, the aerosol optical properties are retained; otherwise, the parameters are adjusted and recalculated. The AOD used for comparison is the MODIS Aerosol Product from the Level 2 (MOD 04) data (Dark Target algorithm) at 500 nm.

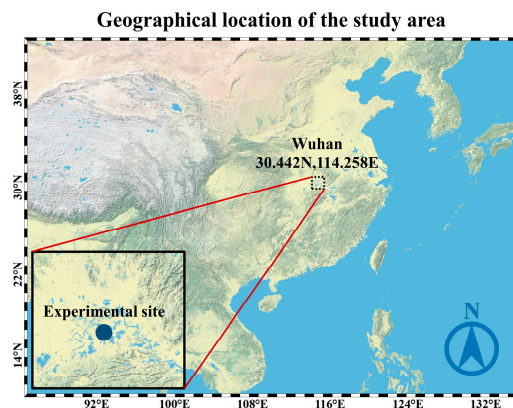


Figure 1. Geographical information and latitude and longitude of the study area.

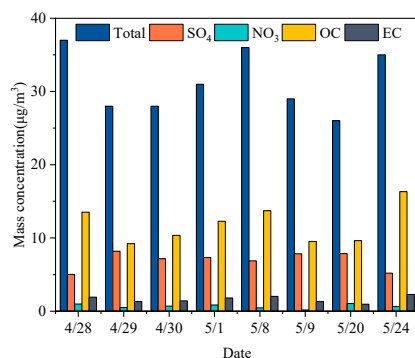


Figure 2. Mass concentrations of $\text{PM}_{2.5}$ and different aerosol types.

2.3. Aerosol Radiation Forcing

Subsequently, the radiative forcing of different aerosol types in Wuhan is simulated using the vector radiative transfer model developed in the previous study [21], and the simulation results are compared and verified using the SBDART (Santa Barbara DISORT Atmospheric Radiative Transfer model) model. The SBDART model is developed based on the discrete coordinate method and the LOWTRAN7 model to deal with various radiative transfer problems in atmospheric energy balance studies [22]. The radiative fluxes at the top of the atmosphere (TOA) and bottom of the atmosphere (BOA) affected by different aerosol types are calculated by aerosol optical properties and radiative transfer model with short-wave radiation at wavelengths of 0.4–3 μm , atmospheric profiles set to mid-latitude summer model, and surface albedo, water vapor concentration and ozone concentration of 0.2, 1.19 g/cm^2 and 0.406 ppm, respectively. Radiative forcing is defined in terms of changes in the net radiative flux due to variations in the atmospheric medium or other climatic perturbations; according to the radiative flux results from the SBDART model, the aerosol direct radiative forcing is calculated as follows,

$$\Delta F = F \downarrow - F \uparrow, \tag{1}$$

$$\Delta F_{aerosol}^{ATM} = \left(\Delta F_{aerosol}^{TOA} - \Delta F_{clear}^{TOA} \right) - \left(\Delta F_{aerosol}^{BOA} - \Delta F_{clear}^{BOA} \right), \tag{2}$$

where Δ represents the difference in radiation flux, the subscripts aerosol and clear represent the case with and without aerosol, respectively, and ATM represents atmospheric

absorption. Further, according to the aerosol radiative forcing, the atmospheric heating rate can be calculated as follows,

$$dT/dt = -(1/\rho c_p) \cdot (d\Delta F_{aerosol}/dz), \tag{3}$$

where c_p represents the constant pressure-specific heat capacity with the value of $1004.67 \text{ Jkg}^{-1}\text{K}^{-1}$, ρ is the air density varying with pressure, z is the altitude, and the atmospheric heating rate dT/dt is in K/day.

3. Results and Discussion

The AOD inversion results of different aerosol types at a wavelength of 500 nm are shown in Figure 3a. The results show that the total aerosol AOD during the test period ranges from 0.19 to 0.39, with an average of about 0.28. The average AOD of SO_4 , NO_3 , OC, and EC are 0.062, 0.008, 0.023, and 0.052, respectively, which account for about 22%, 3%, 8%, and 19% of the total AOD, with SO_4 being the highest and NO_3 the lowest. It can also be found that SO_4/NO_3 does not differ much in MC and AOD, ranging from about 5 to 15, respectively, indicating that the optical properties and radiative effects of these two aerosols are similar. However, OC/EC in AOD (0.3–0.8) is much smaller than MC (6–10), which indicates that EC plays a greater role in the radiation effect.

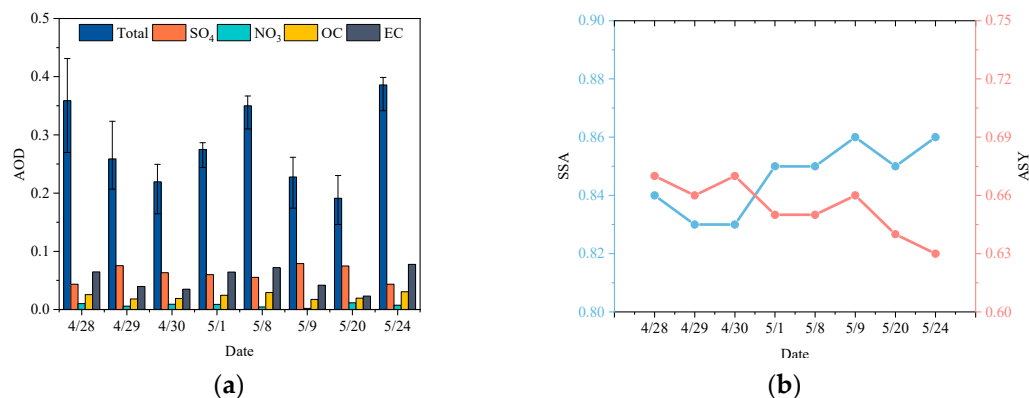


Figure 3. (a) Inversion results of AOD for different aerosol types; (b) Variation of aerosol optical properties with date.

The SSA and ASY of aerosols at different dates are shown in Figure 3b. The results show that the aerosol optical properties change with date, which is due to the change of different aerosol types in the mixed aerosol. From April to May, SSA shows an increasing trend, while ASY shows a decrease. Similar changes have been reported in several studies, with enhanced scattering (decreased absorption) and some decrease in the size of aerosols from spring to summer in Wuhan [23]. However, the optical properties of different aerosol types do not vary much, and the SSA (ASY) of SO_4 , NO_3 , OC, and EC are about 0.98 (0.65), 0.99 (0.65), 0.83 (0.75), and 0.42 (0.35), respectively. SO_4 and NO_3 have the strongest scattering properties, while EC has the strongest absorption properties, and its size is also the smallest.

The results of the radiative forcing simulations for different aerosol types, including TOA, BOA, and ATM, are given in Figure 4a–c. The results show that the aerosol radiative forcing at TOA ranges from about $8\sim 14 \text{ W/m}^2$ with an average of about 10 W/m^2 , while at BOA and ATM ranges from about $-25\sim -55 \text{ W/m}^2$ and $30\sim 70 \text{ W/m}^2$ (average of about -40 and 50 W/m^2), respectively. The radiative forcing of different aerosol types differs significantly. SO_4 and NO_3 have negative radiative forcing in TOA (about $-1\sim -2 \text{ W/m}^2$ and $0\sim -1 \text{ W/m}^2$), indicating a cooling effect on the Earth system by reflecting solar radiation, while OC and EC have positive radiative forcing in TOA, showing a heating effect. Among all aerosol types, EC has the most significant contribution, not only with the largest positive radiative forcing at TOA ($6\sim 18 \text{ W/m}^2$) but also up to 61% and 73% at

BOA and ATM, respectively (10~35 W/m² and 15~55 W/m², respectively), reflecting an extremely strong absorption of radiation. However, the effect of OC, which also plays a heating effect, is much smaller (0~3 W/m² at TOA).

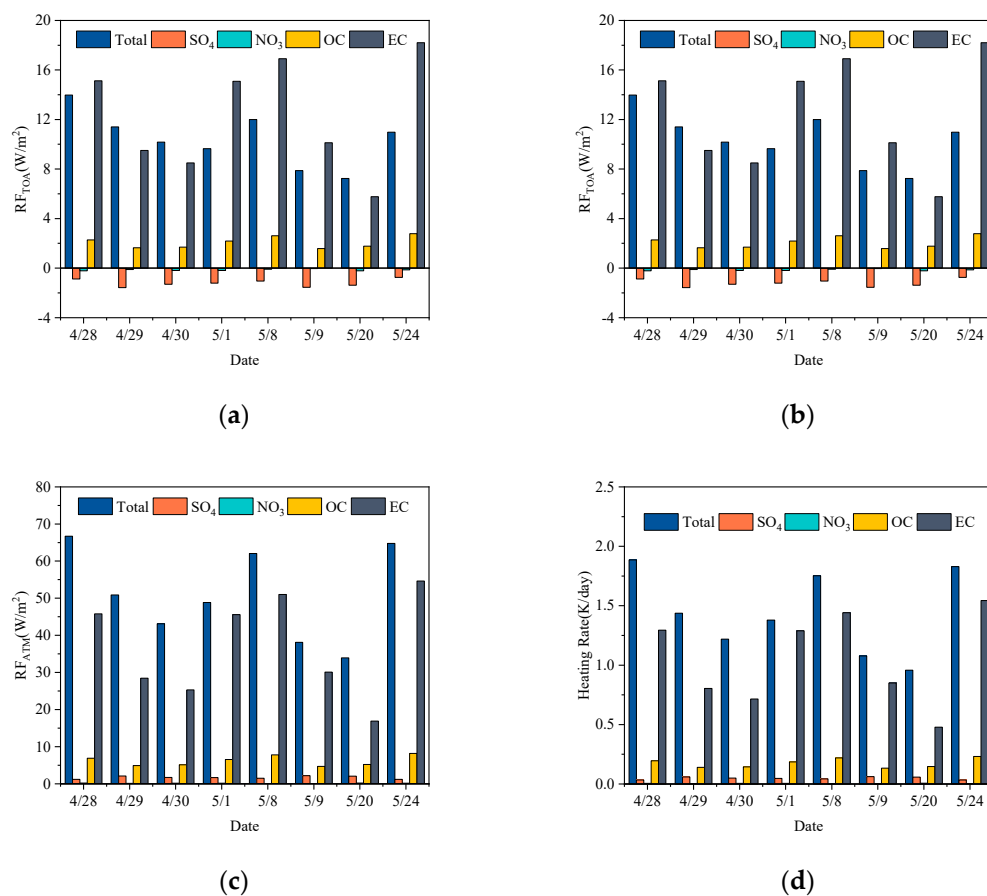


Figure 4. Direct radiative forcing of aerosol types at (a) TOA; (b) BOA; (c) ATM; and (d) Atmospheric heating rates of different aerosol types.

Funding: This research was funded by the National Natural Science Foundation of China (No. 51876147).

Institutional Review Board Statement: Not applicable.

Informed Consent Statement: Not applicable.

Data Availability Statement: The data of this work are freely available from the authors.

Acknowledgments: We acknowledge NASA’s MODIS data. Moreover, an acknowledgment is made to the editors and referees who made important comments to improve this paper.

Conflicts of Interest: The author declares no conflicts of interest.

References

- Climate Change 2014, Synthesis Report, Summary for Policymakers. Available online: https://www.ipcc.ch/pdf/assessment-report/ar5/syr/AR5_SYR_FINAL_SPM.pdf (accessed on 21 April 2022).
- Hui, L.; Liu, X.; Tan, Q.; Feng, M.; An, J.; Qu, Y.; Zhang, N.; Cheng, N. VOC characteristics, sources and contributions to SOA formation during haze events in Wuhan, Central China. *Sci. Total. Environ.* **2019**, *650*, 2624–2639. [\[CrossRef\]](#) [\[PubMed\]](#)
- Bellouin, N.; Quaas, J.; Gryspeerdt, E.; Kinne, S.; Stier, P.; Watson-Parris, D.; Boucher, O.; Carslaw, K.S.; Christensen, M.; Daniau, A.L.; et al. Bounding global aerosol radiative forcing of climate change. *Rev. Geophys.* **2020**, *58*, e2019RG000660. [\[CrossRef\]](#) [\[PubMed\]](#)

4. Hammer, M.S.; Donkelaar, A.; Li, C.; Lyapustin, A.; Sayer, A.M.; Hsu, N.C.; Levy, R.C.; Garay, M.J.; Kalashnikova, O.V.; Kahn, R.A.; et al. Global estimates and long-term trends of fine particulate matter concentrations (1998–2018). *Environ. Sci. Technol.* **2020**, *54*, 7879–7890. [[CrossRef](#)]
5. Xia, X.; Che, H.; Shi, H.; Chen, H.; Zhang, X.; Wang, P.; Goloub, P.; Holben, B. Advances in sunphotometer-measured aerosol optical properties and related topics in China: Impetus and perspectives. *Atmos. Res.* **2021**, *249*, 105286. [[CrossRef](#)] [[PubMed](#)]
6. Pathak, B.; Bhuyan, P.K.; Gogoi, M.; Bhuyan, K. Seasonal Heterogeneity in Aerosol Types Over Dibrugarh-north-eastern India. *Atmos. Environ.* **2012**, *47*, 307–315. [[CrossRef](#)]
7. Choi, Y.; Ghim, Y.S.; Holben, B.N. Identification of Columnar Aerosol Types Under High Aerosol Optical Depth Conditions for a Single Aeronet Site in Korea. *J. Geophys. Res.-Atmos.* **2016**, *121*, 1264–1277. [[CrossRef](#)]
8. Mao, Q.; Huang, C.; Chen, Q.; Zhang, H.; Yuan, Y. Satellite-based identification of aerosol particle species using a 2D-space aerosol classification model. *Atmos. Environ.* **2019**, *219*, 117057. [[CrossRef](#)]
9. Li, K.; Jacob, D.J.; Liao, H.; Zhu, J.; Shah, V.; Shen, L.; Bates, K.H.; Zhang, Q.; Zhai, S. A two-pollutant strategy for improving ozone and particulate air quality in China. *Nat. Geosci.* **2019**, *12*, 906–910. [[CrossRef](#)]
10. Jain, S.; Sharma, S.K.; Vijayan, N.; Mandal, T.K. Seasonal characteristics of aerosols (PM_{2.5} and PM₁₀) and their source apportionment using PMF: A four year study over Delhi, India. *Environ. Pollut.* **2020**, *262*, 114337. [[CrossRef](#)]
11. Daellenbach, K.R.; Uzu, G.; Jiang, J.; Cassagnes, L.E.; Leni, Z.; Vlachou, A.; Stefanelli, G.; Canonaco, F.; Weber, S.; Segers, A.; et al. Sources of particulate-matter air pollution and its oxidative potential in Europe. *Nature* **2020**, *587*, 414–419. [[CrossRef](#)]
12. Chang, X.; Wang, S.; Zhao, B.; Xing, J.; Liu, X.; Wei, L.; Song, Y.; Wu, W.; Cai, S.; Zheng, H.; et al. Contributions of inter-city and regional transport to PM_{2.5} concentrations in the Beijing-Tianjin-Hebei region and its implications on regional joint air pollution control. *Sci. Total. Environ.* **2019**, *660*, 1191–1200. [[CrossRef](#)] [[PubMed](#)]
13. Zheng, H.; Kong, S.; Chen, N.; Yan, Y.; Liu, D.; Zhu, B.; Xu, K.; Cao, W.; Ding, Q.; Lan, B.; et al. Significant changes in the chemical compositions and sources of PM_{2.5} in Wuhan since the city lockdown as COVID-19. *Sci. Total. Environ.* **2020**, *739*, 140000. [[CrossRef](#)] [[PubMed](#)]
14. Huang, F.; Zhou, J.; Chen, N.; Li, Y.; Li, K.; Wu, S. Chemical characteristics and source apportionment of PM_{2.5} in Wuhan, China. *J. Atmos. Chem.* **2019**, *76*, 245–262. [[CrossRef](#)]
15. Liao, W.; Zhou, J.; Zhu, S.; Xiao, A.; Li, K.; Schauer, J.J. Characterization of aerosol chemical composition and the reconstruction of light extinction coefficients during winter in Wuhan, China. *Chemosphere* **2020**, *241*, 125033. [[CrossRef](#)] [[PubMed](#)]
16. Srivastava, A.K.; Mehrotra, B.J.; Singh, A.; Singh, V.; Bisht, D.S.; Tiwari, S.; Srivastava, M.K. Implications of different aerosol species to direct radiative forcing and atmospheric heating rate. *Atmos. Environ.* **2020**, *241*, 117820. [[CrossRef](#)]
17. Ramachandran, S.; Srivastava, R. Mixing states of aerosols over four environmentally distinct atmospheric regimes in Asia: Coastal, urban, and industrial locations influenced by dust. *Environ. Sci. Pollut. R.* **2016**, *23*, 11109–11128. [[CrossRef](#)] [[PubMed](#)]
18. Zhao, H.; Che, H.; Xia, X.; Wang, Y.; Wang, H.; Wang, P.; Ma, Y.; Yang, H.; Liu, Y.; Wang, Y.; et al. Multiyear Ground-Based Measurements of Aerosol Optical Properties and Direct Radiative Effect Over Different Surface Types in Northeastern China. *J. Geophys. Res.-Atmos.* **2018**, *123*, 13887–13916. [[CrossRef](#)]
19. Mao, Q.; Cheng, F.; Chen, M. Experimental Study on the Chemical Characterization of Atmospheric Aerosols in Wuhan, China. *Atmosphere* **2021**, *12*, 1393. [[CrossRef](#)]
20. Hess, M.; Koepke, P.; Schult, I. Optical properties of aerosols and clouds: The software package OPAC. *B Am. Meteorol. Soc.* **1998**, *79*, 831–844. [[CrossRef](#)]
21. Mao, Q.; Nie, X. Polarization performance of a polydisperse aerosol atmosphere based on vector radiative transfer model. *Atmos. Environ.* **2022**, *277*, 119079. [[CrossRef](#)]
22. Ricchiazzi, P.; Yang, S.; Gautier, C.; Sowle, D. SBDART: A research and teaching software tool for plane-parallel radiative transfer in the Earth's atmosphere. *B Am. Meteorol. Soc.* **1998**, *79*, 2101–2114. [[CrossRef](#)]
23. Wang, L.; Gong, W.; Xia, X.; Zhu, J.; Li, J.; Zhu, Z. Long-term observations of aerosol optical properties at Wuhan, an urban site in Central China. *Atmos. Environ.* **2015**, *101*, 94–102. [[CrossRef](#)]

Disclaimer/Publisher's Note: The statements, opinions and data contained in all publications are solely those of the individual author(s) and contributor(s) and not of MDPI and/or the editor(s). MDPI and/or the editor(s) disclaim responsibility for any injury to people or property resulting from any ideas, methods, instructions or products referred to in the content.